

# Universal scaling between precursory duration and event size across mechanically driven geohazards

Qinghua Lei<sup>1\*</sup> and Didier Sornette<sup>2</sup>

<sup>1</sup>*Department of Earth Sciences, Uppsala University, Uppsala, Sweden*

<sup>2</sup>*Institute of Risk Analysis, Prediction and Management, Academy for Advanced Interdisciplinary Studies, Southern University of Science and Technology, Shenzhen, China*

January 2026

## Abstract

Many catastrophic events, including landslides, rockbursts, glacier breakoffs, and volcanic eruptions, are preceded by an observable acceleration phase that offers a critical window for early warning and hazard mitigation; however, the duration of this precursory phase remains poorly constrained across sites, scales, and hazard types. This limitation arises because the onset of acceleration is often identified using heuristic thresholds or empirical criteria. Here, we introduce a physics-based framework that objectively constrains the precursory duration from accelerating dynamics, without prescribing the onset *a priori* or being tied to any specific observable. We analyse a global dataset of 109 geohazard events across seven continents over the past century, quantifying their precursory durations in a consistent manner. For mechanically driven instabilities, we identify a robust scaling between precursory duration and failure volume spanning more than ten orders of magnitude. When expressed in terms of a characteristic system size, this relationship is close to linear, consistent with finite-size scaling near a dynamical critical point. This behaviour indicates that precursory duration reflects the progressive growth of correlated deformation up to system-spanning scales, rather than local rupture kinetics. The resulting universality points to common organising mechanisms governing the approach to catastrophic failure across mechanically driven geohazards.

## Introduction

Forecasting catastrophic events in Earth systems remains challenging despite the widespread availability of high-resolution monitoring data. Across a wide range of geohazards, including landslides, rockbursts, glacier breakoffs, and volcanic eruptions, catastrophic failure is often preceded by a phase of accelerating deformation, seismicity, or other observable precursory signals [1–6]. This precursory phase represents a critical window for early warning, emergency planning, and hazard mitigation. A fundamental yet largely unanswered question is the duration of this phase prior to final failure. Addressing this question is essential for understanding the temporal organisation of failure processes and for constraining the limits of actionable lead time across geohazards.

Despite its central importance, the definition of a precursory phase and its duration remains poorly constrained. In many previous studies, the onset of a precursory phase is often identified using heuristic thresholds, visual inspection, or empirical criteria tied to specific observables, rendering the inferred precursory duration subjective and difficult to compare across events [7–12]. Different choices of observables, smoothing procedures, or reference times can lead to markedly different estimates of when precursory acceleration begins, thereby obscuring any systematic temporal organisation of failure processes. As a result, this ambiguity has so far limited efforts to establish general constraints on precursory duration and to assess whether comparable preparatory processes exist across geohazards.

The precursory dynamics of a heterogeneous system are typically characterised by strong nonlinearity and intermittency, reflecting the presence of positive feedbacks and hierarchically organised damage accumulation as the system approaches failure [13, 14]. These features have been successfully captured by the log-periodic power law singularity (LPPLS) model—a physics-based framework that simultaneously describes both the overall accelerating trend and the superimposed log-periodic organisation of

---

\* Correspondence: [qinghua.lei@geo.uu.se](mailto:qinghua.lei@geo.uu.se)

deformation, reflecting a discrete hierarchy of accelerating instabilities and temporary consolidation as rupture is approached in many geophysical systems [15–20]. The LPPLS model has also been validated using a global dataset of 109 geohazard events [21], encompassing a wide range of hazard types (rockfalls, rockslides, soilslides, hanging glaciers, ice shelves, and volcanic eruptions), observable quantities (displacement, angular change, earthquake count, energy release, rift length, and gas emission), and monitoring approaches (ground-based measurements, remote sensing observations, and seismic/geochemical networks). This validation demonstrates its capability to describe accelerating dynamics across different site settings, spatiotemporal scales, observational resolutions, and hazard types.

Here, we build on this validated framework and dataset to quantify the precursory duration across diverse geohazards. Crucially, we leverage the LPPLS framework to render the concept of precursory duration explicit and operational by endogenising the identification of acceleration onset within the model calibration to monitoring data, rather than prescribing it *a priori*. This enables us to examine how precursory duration scales with event size, revealing a common scaling relationship that links characteristic time and length scales in mechanically driven instabilities. This study focuses on near-surface geohazards, including landslides, rockbursts, glacier breakoffs and volcanic eruptions, for which precursory acceleration is more clearly measurable and physically interpretable owing to shallow sources, spatially constrained rupture zones and dense monitoring. Earthquakes are not considered here, as the generality and interpretation of accelerating seismic release remain debated [22].

## Objective identification of precursory duration across geohazards

We apply the LPPLS framework to four well-instrumented case studies spanning contrasting hazard types, illustrating how precursory duration can be objectively identified from monitored accelerating dynamics. The same analysis is then extended to other cases in the global dataset.

The first case study concerns the Veslemannen landslide in western Norway, a well-instrumented slope instability developed in high-grade metamorphic rocks. This site has been continuously monitored since 2014 using ground-based interferometric synthetic-aperture radar [23], providing displacement measurements with an accuracy of  $\sim 0.5$  mm. In the months leading up to the collapse on 5 September 2019 (failure volume  $\sim 54,000$  m $^3$ ), the landslide exhibited pronounced acceleration punctuated by intermittent deceleration episodes, resulting in cumulative displacements of several metres over a period of  $\sim 3$  months (Fig. 1a shows data from one representative radar point; Extended Data Fig. 1 shows all other radar points). Applying the LPPLS model to the displacement time series captures both the accelerating and oscillatory dynamics characteristic of the precursory phase. Scanning the calibration window reveals a distinct minimum in the regularised cost function (Fig. 1), providing an estimate of the onset time of precursory acceleration on 4 June 2019. The same analysis is performed for all other radar points (Extended Data Fig. 1), with the earliest one (19 May 2019) selected as the onset time for this event. This selected onset time is consistent with the convergence of onset estimates from all radar points that exhibit a stable plateau after August 2019 (Extended Data Fig. 2a), demonstrating the robustness of the identified precursory onset. The interval between the onset and failure times then defines the precursory duration, which is 109 days.

The second case study examines a rockburst event that occurred in an underground coal mine in New South Wales, Australia. This mine, located at a depth of  $\sim 250$  m and excavated using the longwall mining method, was instrumented with multipoint extensometers (with an accuracy of  $\sim 0.5$  mm) to continuously monitor roof displacement within a gateroad [24]. In the days preceding the roof collapse at 13:35 on 4 June 2004, the displacement time series exhibited a clear acceleration punctuated by intermittent deceleration episodes (Fig. 1b), indicative of an evolving instability. The LPPLS model captures both the acceleration and oscillation patterns characteristic of the precursory phase. A pronounced minimum in the regularised cost function indicates an onset of acceleration at 2:00 on 2 June 2004 (Fig. 1b), supported by the convergence of onset estimates towards stable plateaus (Extended Data Fig. 2b), implying a precursory duration of  $\sim 2.5$  days. The associated failure volume is estimated to be  $\sim 50$  m $^3$ , based on the dimensions of the gateroad (5.2 m in width and 3 m in height).

The third case study regards a hanging cold glacier located on the south face of the Grandes Jorasses massif, Italy, at an elevation of  $\sim 3,950$  m above sea level [6]. Surface displacements were monitored using a robotic total station equipped with multiple reflectors, providing measurements with an accuracy of  $\sim 1$  cm. In 2014, a large ice volume of  $\sim 1.05 \times 10^5$  m $^3$  detached in two consecutive breakoff events [25] on September 23 and 29. In the months preceding the final event, the glacier exhibited a smooth, sustained acceleration in surface displacement that is well captured by the LPPLS model (Fig. 1c). A clear minimum in the regularised cost function identifies the onset of acceleration in late March 2014,

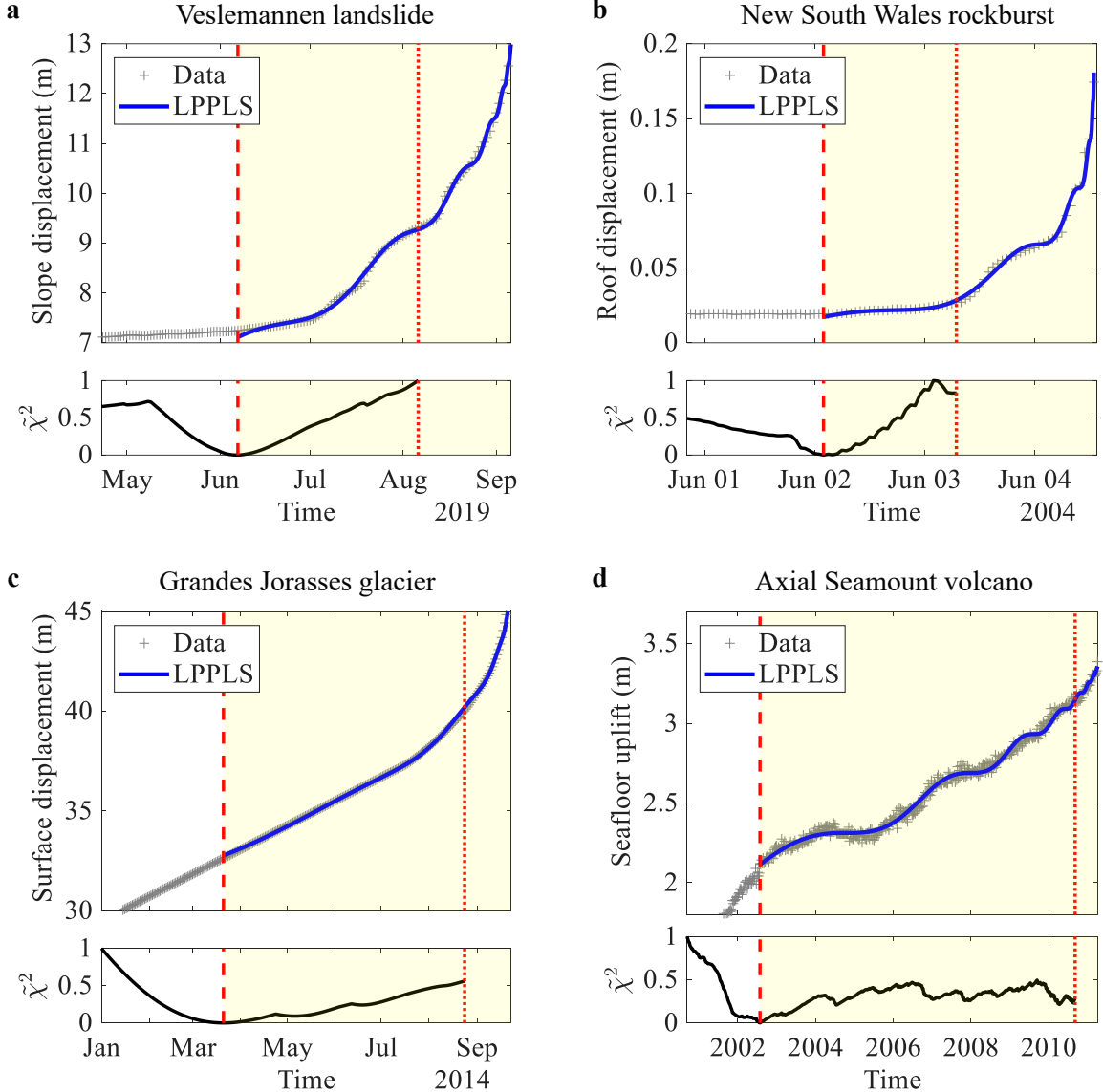


**Fig. 1| Representative examples of precursory dynamics and onset identification across geohazards.** In each subfigure, the upper panel shows the monitoring data (grey symbols) together with the corresponding LPPLS model fit (blue line), while the lower panel shows the normalised regularised cost function  $\tilde{\chi}^2$  as a function of the calibration window start time  $\tau$ . Vertical dashed lines indicate the identified onset time  $\tau^*$  of precursory acceleration, vertical dotted lines mark the latest time of the  $\tau$ -scanning interval, and shaded regions highlight the inferred precursory phase. The examples include: (a) slope surface displacement (daily aggregation) prior to the catastrophic landslide on 5 September 2019, at Veslemannen, Norway; (b) tunnel roof displacement (hourly aggregation) prior to a violent rockburst on 4 June 2004, in an underground coal mine in New South Wales, Australia; (c) glacier surface displacement (daily aggregation) prior to rapid breakoffs in late September 2014, at the Grandes Jorasses glacier, Italy; and (d) seafloor uplift (weekly aggregation) prior to the volcanic eruption on 6 April 2011, at Axial Seamount, Pacific Ocean.

corresponding to a precursory duration of  $\sim 6$  months. The inferred onset time exhibits a stable plateau from late August 2014 onward, indicating robust identification of the precursory onset (Extended Data Fig. 2c).

The fourth case study focuses on Axial Seamount, an active submarine volcano located  $\sim 500$  km offshore Oregon, USA, whose summit caldera lies at a water depth of about 1.5 km. Axial Seamount has been continuously monitored since 1998 by a cabled seafloor observatory, which records vertical seafloor deformation with a resolution of  $\sim 1$  cm using bottom pressure recorders [26]. We focus on the eruption that occurred in April 2011, prior to which the volcano exhibited a prolonged sequence of inflation–deflation cycles spanning more than eight years [27] (Fig. 1d). The erupted magma volume associated with the 2011 event is  $\sim 9.9 \times 10^7 \text{ m}^3$ . The seafloor uplift time series is well described by the LPPLS model, capturing the long-term acceleration together with the superimposed oscillations characteristic of episodic magma pressurisation and release during volcanic unrest. A well-defined minimum in the regularised cost function identifies the onset of precursory acceleration in 2002, yielding a precursory duration of  $\sim 8.7$  years. The inferred onset time is already detectable prior to 2007 and, despite fluctuations between 2007 and 2010, stabilises thereafter, indicating robust identification of the precursory onset (Extended Data Fig. 2d).

The four case studies presented above form part of a larger global dataset comprising 109 geohazard events, including landslides, rockbursts, glacier breakoffs, and volcanic eruptions, distributed across seven continents (Fig. 2). The same LPPLS-based framework is applied consistently to all events in the dataset to identify their onset times and precursory durations. Details of the full dataset, including event locations, hazard types, data sources, failure volumes, and precursory durations, are provided in the Supplementary Information.

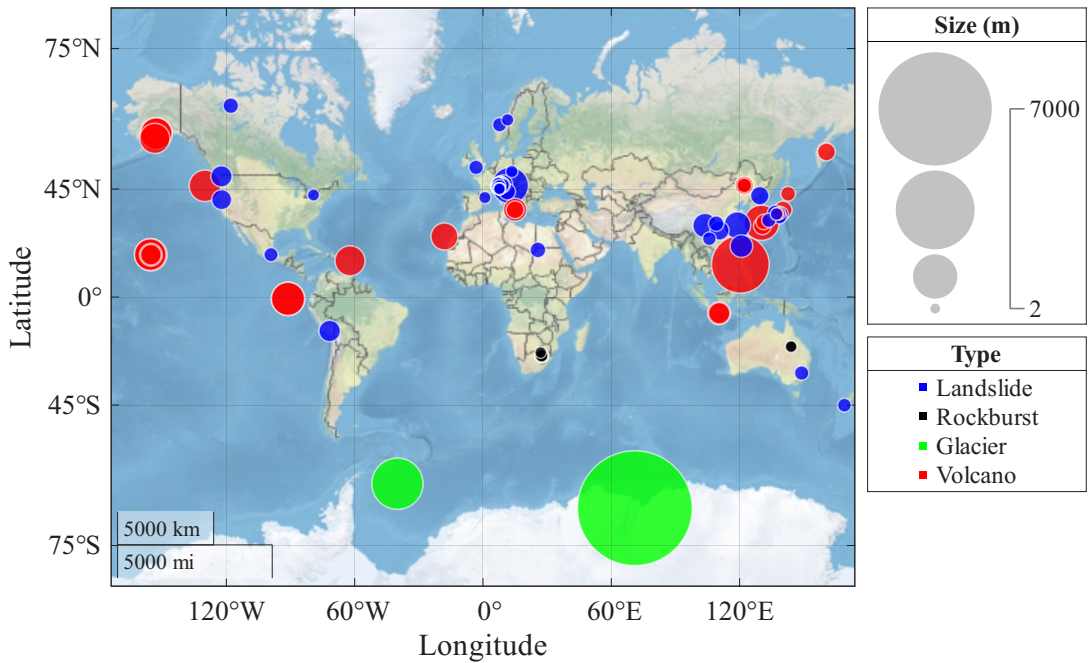


**Fig. 2 | Global distribution of 109 historical geohazard events.** The dataset includes 49 landslides, 11 rockbursts, 17 glacier breakoffs, and 32 volcanic eruptions. Colours indicate hazard type and symbol size scales with the cube root of failure volume.

## Scaling between precursory duration and failure volume

We perform a correlation analysis between precursory duration  $T$  and failure volume  $V$  across the global dataset of 109 geohazard events. When volcanic eruptions are excluded, the remaining mechanically driven instabilities, including landslides, rockbursts, and glaciers, exhibit a systematic scaling between precursory duration and failure volume (Fig. 3). Despite spanning more than ten orders of magnitude in failure volume and encompassing diverse hazard types, the data collapse onto a clear scaling trend (Fig. 3). A log–log regression yields a power law relation  $T \propto V^\zeta$ , with  $\zeta = 0.35 \pm 0.05$  (Fig. 3). The

statistical significance of the observed scaling is supported by multiple complementary statistical tests (Supplementary Note S3 and Supplementary Table S5), all of which decisively reject the null hypothesis of no dependence between  $T$  and  $V$ .

When analysed by hazard type (Supplementary Table S5), landslides, glaciers, and rockbursts yield scaling exponents that cluster within  $\zeta = 0.30 \pm 0.10$ , broadly consistent with the exponent obtained for the combined dataset of mechanically driven instabilities, although the rockburst estimate remains statistically inconclusive, likely owing to limited sample size. Volcanic eruptions, by contrast, do not exhibit a comparable dependence of precursory duration on failure volume: their fitted exponent is close to zero, and the null hypothesis of no scaling cannot be rejected (Supplementary Table S5). Notably, although volcanic eruptions do not exhibit a significant scaling, their precursory durations largely fall within the confidence bounds of the scaling derived from mechanically driven instabilities (Extended Data Fig. 3), indicating compatibility with the overall trend despite the lack of a clear correlation. Taken together, these results demonstrate a statistically robust scaling between precursory duration and failure volume for mechanically driven geohazards, while delineating volcanic eruptions as a distinct class in which failure volume is not the primary control on precursory timescales.

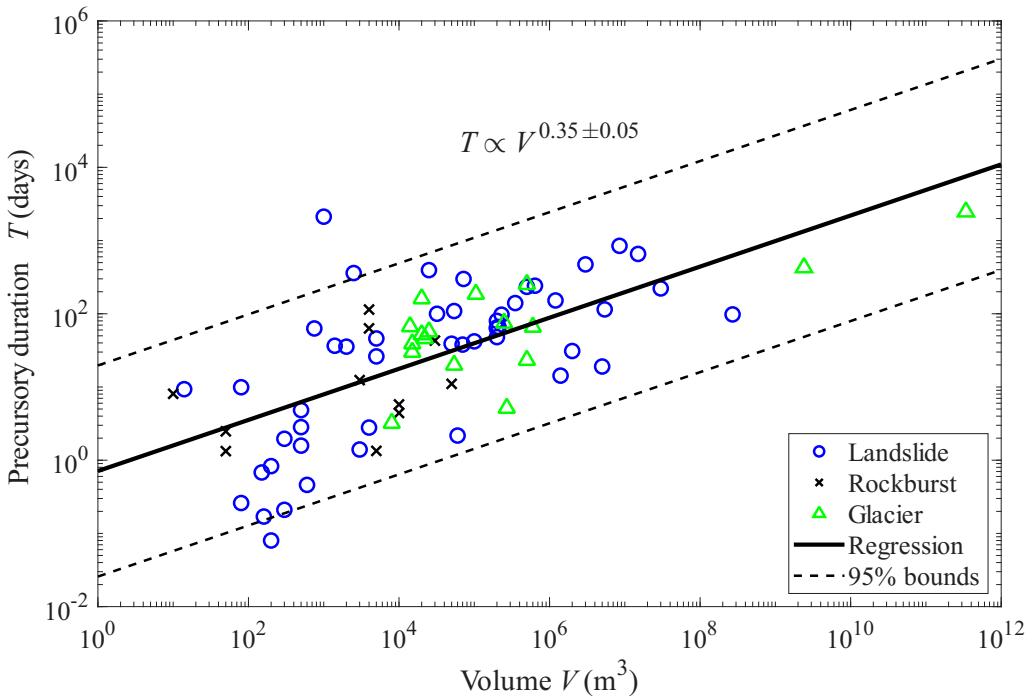


**Fig. 3| Scaling relationship between precursory duration  $T$  and failure volume  $V$  for mechanically driven geohazards.** Symbols indicate hazard type, the solid black line shows the best-fit power law regression  $T \propto V^{0.35 \pm 0.05}$ , and dashed lines mark the 95% confidence interval.

## Organising mechanisms across geohazards

Our analysis reveals a clear empirical scaling between precursory duration and failure volume across mechanically driven geohazards,  $T \propto V^{0.35}$ , which implies  $T \propto L^{1.05}$  when expressing volume in terms of a characteristic system size  $L \sim V^{1/3}$ . This scaling behaviour implies an “effective” preparatory rate, defined as  $\gamma^* = L/T$ , characterising the pace at which instability progressively organises across a finite system. From the observed scaling, we estimate  $\gamma^*$  to be  $\sim 0.85$  m/day, with a 95% confidence interval spanning approximately 0.03 to 23 m/day. This variability is expected and reflects differences in system geometry, material properties, and loading conditions. Notably, this scaling emerges only when precursory duration is defined consistently within a unified, physics-based framework, rather than through heuristic or subjective criteria commonly used in previous studies [7–12].

The observed near-linear  $L$ - $T$  scaling admits a natural interpretation within the framework of dynamical critical phenomena and finite-size scaling. Catastrophic failure can be viewed as a critical point marking the transition from a quasi-static creep regime to an elasto-dynamic rupture regime, culminat-

ing in system-wide collapse [13, 14, 28–30]. As a system approaches the critical rupture time  $t_c$ , it is characterised by the progressive development of correlated clusters of damage and/or slip, quantified by a correlation length  $\xi$  and an associated correlation time  $\Upsilon$ , which sets the characteristic timescale of fluctuations and precursory activity [31–35]. For idealised infinite systems, these two quantities diverge as power laws of the distance to criticality [36–38]:  $\xi(t) \sim (t_c - t)^{-\nu}$  and  $\Upsilon(t) \sim (t_c - t)^{-\mu}$ , where  $\nu$  and  $\mu$  are the critical exponents governing spatial and temporal correlations, respectively. These divergences can be compactly summarised by the dynamic scaling relation  $\Upsilon \sim \xi^z$ , where  $z = \mu/\nu$  is the dynamic critical exponent. However, real geophysical systems are finite. Finite-size scaling theory predicts that the divergence of  $\xi$  cannot continue indefinitely: as  $t \rightarrow t_c$ ,  $\xi$  saturates at the characteristic system size, i.e.  $\xi \lesssim L$ . By the same reasoning, the correlation time also saturates at a finite value controlled by the system size,  $\Upsilon \sim \xi^z \lesssim L^z$ , such that the maximal observable precursory duration is set by this finite-size cutoff.

Our empirically observed near-linear  $L$ – $T$  relation therefore corresponds to a dynamic exponent  $z \approx 1$ , implying that temporal and spatial correlations grow approximately proportionally as instability organises towards system-spanning rupture. In this finite-size criticality view, the precursory phase reflects the approach to a critical point whose apparent “duration” is determined by the time required for correlations to reach the system scale. This perspective contrasts with traditional views in which precursory duration is controlled by local fracturing or sliding rates, as emphasised in subcritical crack growth [39] and rate-and-state friction [40], and instead highlights the dominant role of system-scale organisation in setting precursory timescales. Such behaviour is consistent with rupture processes governed by long-range interactions, where stress perturbations are transmitted efficiently across the system [35, 41]. The growth of correlations is not diffusive but occurs through cascades of interacting local instabilities, leading to hierarchical organisation and intermittent activity [14, 42]. The LPPLS framework, which captures both accelerating and oscillatory dynamics, is consistent with this picture, reflecting the coexistence of positive feedback arising from amplified interactions across scales and hierarchically organised damage/slip processes that evolve intermittently as failure is approached [21, 43].

Under this interpretation, the near-linear scaling between precursory duration and system size reflects the time required for instability to organise at the system scale, rather than the rate of rupture propagation. Accordingly, precursory duration is primarily constrained by system size, even though the underlying deformation and rupture processes remain highly nonlinear and intermittent. This scaling is therefore expected for geohazards in which failure develops through progressive damage accumulation within a finite source region, including landslides, rockbursts, and glaciers. The absence of a significant scaling for volcanic eruptions is also physically informative, consistent with the fact that volcanic unrest is commonly controlled by magma transport, pressurisation, phase changes, and evolving rheology [44], processes that do not necessarily involve a progressive, system-wide build-up of mechanically correlated deformation within a fixed source volume. Overall, our results identify this scaling as a robust signature of finite-size criticality in a broad class of mechanically driven instabilities, with important implications for geohazard mitigation.

## Methods

### Log-periodic power law singularity model

We use the log-periodic power law singularity (LPPLS) model to describe precursory dynamics in geophysical systems. The first-order expression of the LPPLS formulation is given by [15, 21]:

$$\Omega(t) = A + B(t_c - t)^m + C(t_c - t)^m \cos[\omega \ln(t_c - t) - \phi], \quad m < 1, \quad (1)$$

where  $\Omega$  denotes the observable quantity (e.g. displacement, strain, energy release, earthquake count, or gas emission),  $t$  is time,  $t_c$  is the critical time,  $m$  is the critical exponent,  $\omega$  is the angular log-periodic frequency,  $\phi$  is a phase shift, and  $A$ ,  $B$ , and  $C$  are constants. Thus, the LPPLS model involves seven parameters  $\Theta = \{t_c, m, \omega, \phi, A, B, C\}$ . It captures power law acceleration towards a finite-time singularity, modulated by log-periodic oscillations associated with discrete scale invariance and intermittent rupture processes in heterogeneous materials [18–20, 43].

### Lagrange regularisation approach

To determine precursory duration, we calibrate the LPPLS model (see Supplementary Note S1) to time series of observations  $\Omega(t_i)$  recorded at times  $t_i \in [t_0, t_{\text{end}}]$ , with  $i = 1, \dots, N$ , where  $N$  is the total

number of time stamps, and  $t_0$  and  $t_{\text{end}}$  respectively denote the start and end times of the observational record. Importantly, the early portion of the time series may reflect dynamics unrelated to the precursory activity and therefore does not necessarily fall within the accelerating regime described by the LPPLS model. To objectively identify the onset of the acceleration, we adopt the Lagrange regularisation approach [45, 46], where the starting time  $\tau$  is treated as an endogenous variable and determined by minimising a regularised cost function:

$$\chi^2(\tau, \theta) = \frac{r^2(\tau, \theta)}{n - p} - \lambda \tau, \quad (2)$$

where  $p = 7$  is the number of LPPLS model parameters,  $n$  is the number of observations within the window  $[\tau, t_{\text{end}}]$ ,  $r^2$  is the sum of squared residuals of the LPPLS fit over this window, and  $\lambda$  is a Lagrange multiplier controlling the trade-off between goodness of fit and window length. For each candidate  $\tau$ , the LPPLS model is calibrated over the interval  $[\tau, t_{\text{end}}]$  using a stable and robust fitting scheme [47], with the minimised  $r^2$  further substituted into equation (2) to evaluate the regularised cost function. In our implementation, the Lagrange multiplier  $\lambda$  is estimated as the slope in a linear regression of  $r^2$  with respect to  $\tau$ . We scan  $\tau$  over the interval from  $t_0$  up to the latest time for which at least 30 data points remain available for calibration. The optimal value  $\tau^*$ , which minimises  $\chi^2$ , is identified as the onset time, and the precursory duration is then estimated as  $T = t_{\text{end}} - \tau^*$ . For presentation purposes, we compute a normalised regularised cost function  $\tilde{\chi}^2$ , by rescaling  $\chi^2$  using its minimum and maximum values over the scanned range of  $\tau$ ; this normalisation does not affect the identification of  $\tau^*$ .

The Lagrange regularisation approach admits a natural interpretation from the perspective of statistical physics [48, 49]. Specifically, fixing the calibration window length is analogous to working in a canonical ensemble with a fixed number of degrees of freedom, whereas allowing the window start time to vary corresponds to a grand canonical ensemble in which the number of data points is free but incurs an effective cost controlled by the Lagrange multiplier  $\lambda$ . In this analogy,  $\lambda$  plays a role similar to a chemical potential that counteracts the intrinsic bias towards short windows. Shorter windows yield better fits, not because they are more informative, but because a fixed number of parameters is calibrated on fewer data points. The Lagrange multiplier term  $\lambda$  therefore penalises excessively short windows, preventing a systematic bias towards them and enabling an objective identification of the onset of the precursory phase without imposing it *a priori*.

## Acknowledgements

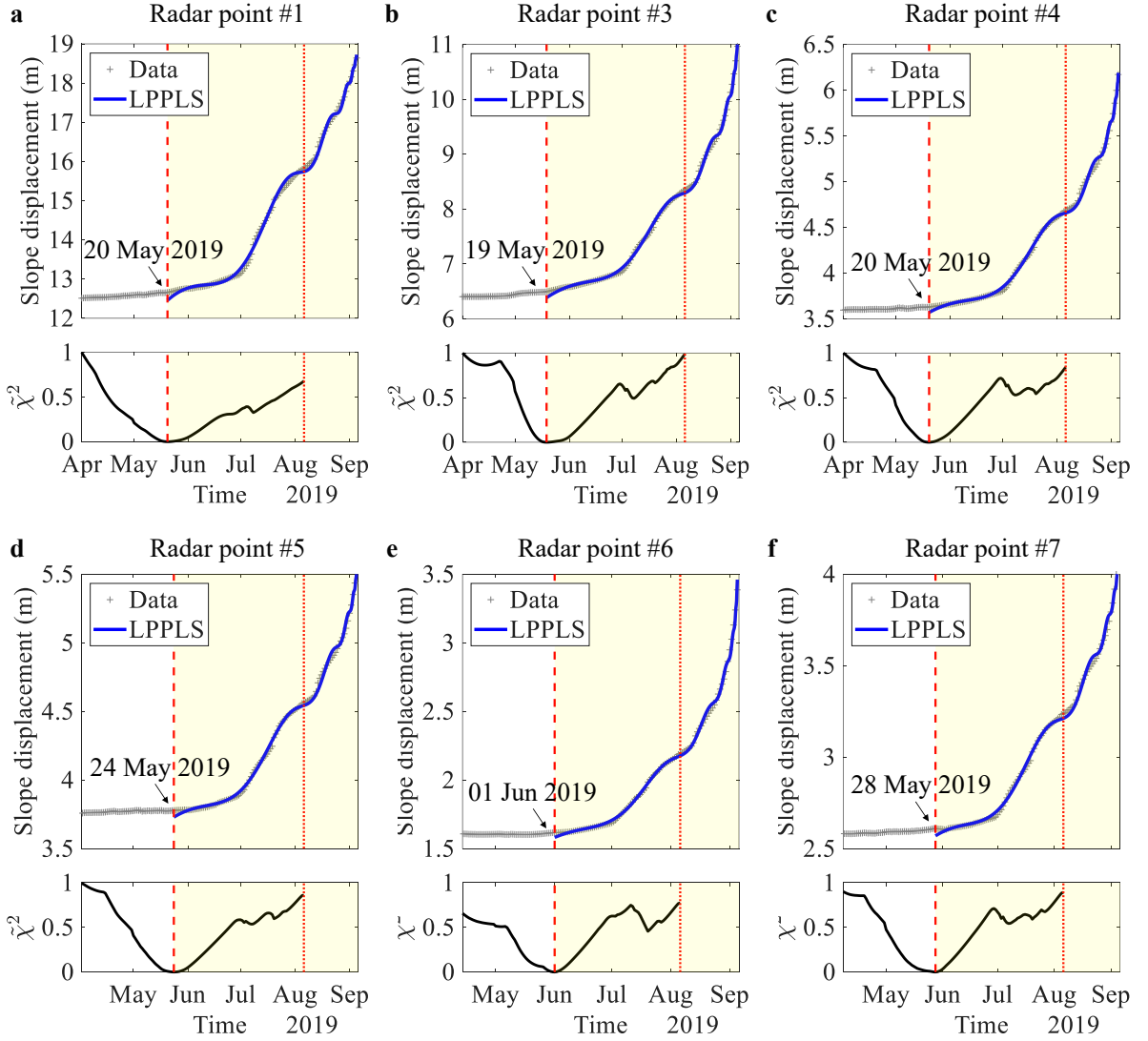
Q.L. is grateful for support from the European Research Council (ERC) under the European Union’s Horizon Europe programme (ERC Consolidator Grant, grant no. 101232311) for the project “Unified framework for modelling progressive to catastrophic failure in fractured media (FORECAST)”. Q.L. and D.S. acknowledge support from Norwegian Water Resources and Energy Directorate for funding the project “Towards a Next-Generation Landslide Early Warning System”. D.S. is grateful for partial support from the National Natural Science Foundation of China (Grant No. U2039202, T2350710802), from the Shenzhen Science and Technology Innovation Commission (Grant No. GJHZ20210705141805017) and the Center for Computational Science and Engineering at the Southern University of Science and Technology.

## Author contributions

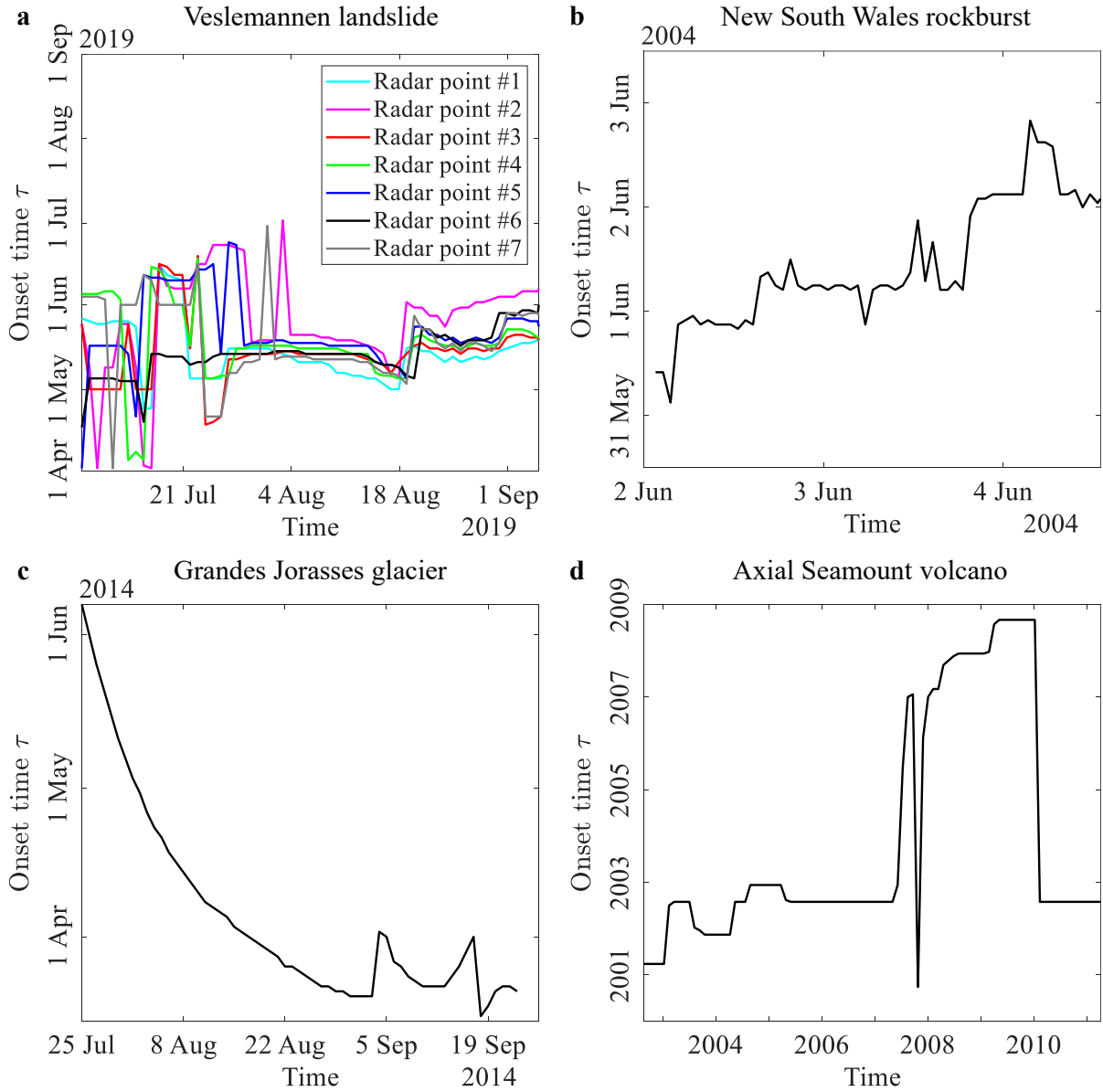
Q.L. conceived the study, performed the analysis, and wrote the manuscript. Q.L. and D.S. devised the method and interpreted the results. D.S. reviewed and edited the manuscript.

## Data availability

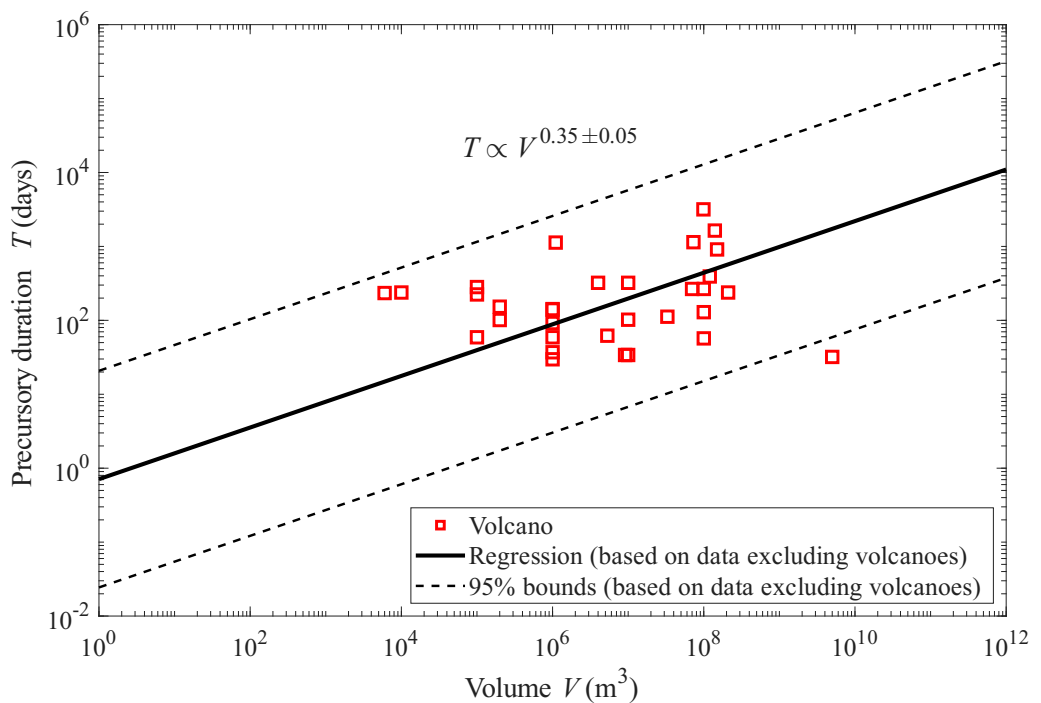
No new data were produced in this work. All data underlying this study were obtained from previously published sources, with full details and references provided in the Supplementary Information. The code used in this study is available at Zenodo: <https://doi.org/10.5281/zenodo.15362582>.



**Extended Data Fig. 1 | Precursory dynamics and onset identification for the Veslemannen landslides based on different radar point measurements.** In each subfigure, the upper panel shows the monitoring data (grey symbols) together with the corresponding LPPLS fit (blue line), while the lower panel shows the normalised regularised cost function  $\tilde{\chi}^2$  as a function of the calibration window start time  $\tau$ . Vertical dashed lines indicate the identified onset time  $\tau^*$  of the precursory phase, vertical dotted lines mark the latest time of the  $\tau$ -scanning interval, and shaded regions highlight the inferred precursory phase.



**Extended Data Fig. 2 | Temporal evolution of the inferred onset time of precursory phase.** The inferred onset time  $\tau$  is shown as a function of the end time of the calibration window used for LPPLS fitting. Panels show examples for (a) the Veslemannen landslide, (b) the New South Wales rockburst, (c) the Grandes Jorasses glacier, and (d) the Axial Seamount volcano.



**Extended Data Fig. 3 | Comparison of volcanic precursory durations with scaling derived from mechanically driven geohazards.** The solid black line shows the scaling relationship between precursory duration and failure volume derived from the combined dataset of landslides, rockbursts, and glaciers, with dashed lines indicating the 95% confidence interval.

## References

- [1] Lacroix, P., Handwerger, A. L. & Bièvre, G. Life and death of slow-moving landslides. *Nat. Rev. Earth Environ.* **1**, 404–419 (2020).
- [2] Feng, X.-T. et al. Monitoring, warning, and control of rockburst in deep metal mines. *Engineering* **3**, 538–545 (2017).
- [3] Acocella, V. et al. Towards scientific forecasting of magmatic eruptions. *Nat. Rev. Earth. Environ.* **5**, 5–22 (2023).
- [4] Lei, Q., Sornette, D., Yang, H. & Loew, S. Real-time forecast of catastrophic landslides via dragon-kings detection. *Geophys. Res. Lett.* **50**, e2022GL100832 (2023).
- [5] Lei, Q. & Sornette, D. Endo-exo framework for a unifying classification of episodic landslide movements: Implications for forecasting catastrophic failures. *Sci. Adv.* (2025).
- [6] Faillettaz, J., Funk, M. & Vincent, C. Avalanching glacier instabilities: Review on processes and early warning perspectives. *Rev. Geophys.* **53**, 203–224 (2015).
- [7] Passarelli, L. & Brodsky, E. E. The correlation between run-up and repose times of volcanic eruptions. *Geophys. J. Int.* **188**, 1025–1045 (2012).
- [8] Phillipson, G., Sobradelo, R. & Gottsmann, J. Global volcanic unrest in the 21st century: An analysis of the first decade. *J. Volcanol. Geotherm. Res.* **264**, 183–196 (2013).
- [9] Crosta, G. B. et al. Long-term evolution and early warning strategies for complex rockslides by real-time monitoring. *Landslides* **14**, 1615–1632 (2017).
- [10] Askaripour, M. et al. Rockburst in underground excavations: A review of mechanism, classification, and prediction methods. *Undergr. Space* **7**, 577–607 (2022).
- [11] Leinauer, J. et al. An approach for prospective forecasting of rock slope failure time. *Commun. Earth Environ.* **4**, 253 (2023).
- [12] Feng, B. et al. Acceleration stage detection and dynamic model selection for real-time landslide time-of-failure predictions. *Acta Geotech.* (2025).
- [13] Johansen, A. & Sornette, D. Critical ruptures. *Eur. Phys. J. B* **18**, 163–181 (2000).
- [14] Sornette, D. Predictability of catastrophic events: Material rupture, earthquakes, turbulence, financial crashes, and human birth. *Proc. Natl. Acad. Sci.* **99**, 2522–2529 (2002).
- [15] Sornette, D. & Sammis, C. G. Complex critical exponents from renormalization group theory of earthquakes: Implications for earthquake predictions. *J. Phys. I France* **5**, 607–619 (1995).
- [16] Ouillon, G. & Sornette, D. The concept of ‘critical earthquakes’ applied to mine rockbursts with time-to-failure analysis. *Geophys. J. Int.* **143**, 454–468 (2000).
- [17] Faillettaz, J. et al. Evidence of log-periodic oscillations and increasing icequake activity during the breaking-off of large ice masses. *J. Glaciol.* **54**, 725–737 (2008).
- [18] Lei, Q. & Sornette, D. Log-periodic signatures prior to volcanic eruptions: evidence from 34 events. *Earth Planet. Sci. Lett.* **666**, 119496 (2025).
- [19] Lei, Q. & Sornette, D. Log-periodic power law singularities in landslide dynamics: Statistical evidence from 52 crises. *Geophys. Res. Lett.* **52**, e2025GL116379 (2025).
- [20] Lei, Q. & Sornette, D. Oscillatory finite-time singularities in rockbursts. *Int. J. Rock Mech. Min. Sci.* **192**, 106156 (2025).
- [21] Lei, Q. & Sornette, D. Unified failure model for landslides, rockbursts, glaciers, and volcanoes. *Commun. Earth Environ.* **6**, 390 (2025).
- [22] Mignan, A. Retrospective on the Accelerating Seismic Release (ASR) hypothesis: Controversy and new horizons. *Tectonophysics* **505**, 1–16 (2011).

[23] Kristensen, L. et al. Movements, failure and climatic control of the Veslemannen rockslide, Western Norway. *Landslides* **18**, 1963–1980 (2021).

[24] Shen, B., King, A. & Guo, H. Displacement, stress and seismicity in roadway roofs during mining-induced failure. *Int. J. Rock Mech. Min. Sci.* **45**, 672–688 (2008).

[25] Faillettaz, J., Funk, M. & Vagliasindi, M. Time forecast of a break-off event from a hanging glacier. *The Cryosphere* **10**, 1191–1200 (2016).

[26] Chadwick, W. W. et al. Geodetic monitoring at Axial Seamount since its 2015 eruption reveals a waning magma supply and tightly linked rates of deformation and seismicity. *Geochem. Geophys. Geosyst.* **23**, e2021GC010153 (2022).

[27] Chadwick, W. W., Nooner, S. L., Butterfield, D. A. & Lilley, M. D. Seafloor deformation and forecasts of the April 2011 eruption at Axial Seamount. *Nat. Geosci.* **5**, 474–477 (2012).

[28] Bonamy, D. & Bouchaud, E. Failure of heterogeneous materials: A dynamic phase transition? *Phys. Rep.* **498**, 1–44 (2011).

[29] Rundle, J. B. et al. Statistical physics approach to understanding the multiscale dynamics of earthquake fault systems. *Rev. Geophys.* **41**, 2003RG000135 (2003).

[30] Vu, C.-C. et al. Compressive failure as a critical transition: Experimental evidence and mapping onto the universality class of depinning. *Phys. Rev. Lett.* **122**, 015502 (2019).

[31] Alava, M. J., Nukala, P. K. V. V. & Zapperi, S. Statistical models of fracture. *Adv. Phys.* **55**, 349–476 (2006).

[32] Girard, L., Amitrano, D. & Weiss, J. Failure as a critical phenomenon in a progressive damage model. *J. Stat. Mech.* **2010**, P01013 (2010).

[33] Pradhan, S., Hansen, A. & Chakrabarti, B. K. Failure processes in elastic fiber bundles. *Rev. Mod. Phys.* **82**, 499–555 (2010).

[34] Sornette, D. *Critical Phenomena in Natural Sciences – Chaos, Fractals, Selforganization and Disorder: Concepts and Tools*. (Springer, 2006).

[35] Sornette, D. & Andersen, J. V. Scaling with respect to disorder in time-to-failure. *Eur. Phys. J. B* **1**, 353–357 (1998).

[36] Cardy, J. *Scaling and Renormalization in Statistical Physics*. (Cambridge University Press, 1996).

[37] Henkel, M., Hinrichsen, H. & Lübeck, S. *Non-Equilibrium Phase Transitions*, Vol. 1. (Springer, 2008).

[38] Privman, V. (ed.) *Finite Size Scaling and Numerical Simulation of Statistical Systems*. (World Scientific, 1990).

[39] Brantut, N. et al. Time-dependent cracking and brittle creep in crustal rocks: A review. *J. Struct. Geol.* **52**, 17–43 (2013).

[40] Marone, C. Laboratory-derived friction laws and their application to seismic faulting. *Annu. Rev. Earth Planet. Sci.* **26**, 643–696 (1998).

[41] Kawamura, H. et al. Statistical physics of fracture, friction, and earthquakes. *Rev. Mod. Phys.* **84**, 839–884 (2012).

[42] Ben-Zion, Y. Collective behavior of earthquakes and faults: Continuum–discrete transitions, progressive evolutionary changes, and different dynamic regimes. *Rev. Geophys.* **46**, 2008RG000260 (2008).

[43] Sornette, D. Discrete-scale invariance and complex dimensions. *Phys. Rep.* **297**, 239–270 (1998).

[44] Caricchi, L. et al. The build-up and triggers of volcanic eruptions. *Nat. Rev. Earth. Environ.* **2**, 458–476 (2021).

- [45] Demos, G. & Sornette, D. Birth or burst of financial bubbles: which one is easier to diagnose? *Quant. Finance* **17**, 657–675 (2017).
- [46] Demos, G. & Sornette, D. Comparing nested data sets and objectively determining financial bubbles' inceptions. *Physica A* **524**, 661–675 (2019).
- [47] Filimonov, V. & Sornette, D. A stable and robust calibration scheme of the log-periodic power law model. *Physica A* **392**, 3698–3707 (2013).
- [48] Gibbs, J. W. *Elementary Principles in Statistical Mechanics*. (Charles Scribner's Sons, 1902).
- [49] Callen, H. B. *Thermodynamics and an Introduction to Thermostatistics*, 2nd ed. (John Wiley & Sons, 1985).